ACS APPLIED MATERIALS & INTERFACES

Research Article

www.acsami.org

$NiSe_2$ Nanooctahedra as an Anode Material for High-Rate and Long-Life Sodium-Ion Battery

Shaohua Zhu,[†] Qidong Li,[†] Qiulong Wei,*[,†] Ruimin Sun,[†] Xiaoqing Liu,[‡] Qinyou An,[†] and Liqiang Mai*[,†]

[†]State Key Laboratory of Advanced Technology for Materials Synthesis and Processing, Wuhan University of Technology, Wuhan 430070, China

[‡]Center of Materials Research and Testing, Wuhan University of Technology, Wuhan 430070, China

Supporting Information

ABSTRACT: In this article, we report $NiSe_2$ nanooctahedra as a promising anode material for sodium-ion batteries (SIBs). They exhibit outstanding long-term cyclic stability (313 mAh/g after 4000 cycles at 5 A/g) and excellent high-rate capability (175 mAh/g at 20 A/g). Besides, the initial Coulombic efficiency of $NiSe_2$ is also very impressive (over 90%). Such remarkable performances are attributed to good conductivity, structural stability, and the pseudocapacitive behavior of the $NiSe_2$. Furthermore, the sodium ion storage mechanism of $NiSe_2$ is first investigated by *in situ* XRD and *ex situ* XRD. These highlights give $NiSe_2$ a competitive strength for rechargeable SIBs.

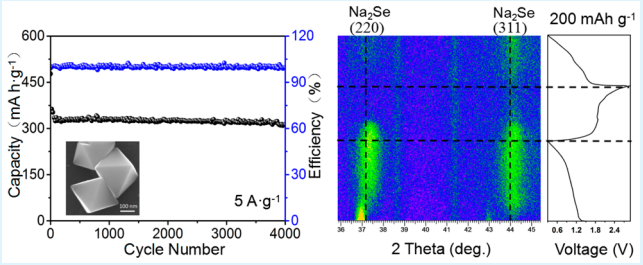

KEYWORDS: *sodium-ion batteries, $NiSe_2$ nanooctahedra, anode, high-rate, long-term cycle life*

INTRODUCTION

Rechargeable lithium-ion batteries (LIBs) have been widely investigated and successfully commercialized due to their high energy density and outstanding cycling stability.[1,2] However, high cost and the limited lithium supplies restrict their development. Recently, sodium-ion batteries (SIBs) have attracted extensive attention, because of the low cost and abundance of sodium resource in comparison to lithium.[3−8] Nevertheless, the ionic radius and molar mass of sodium are larger than those of lithium, which lead to larger volume change and poorer electrochemical performance.[9−11] Thus, it is urgent to exploit new electrode materials with high performance for suitable Na-host materials to accommodate reversible sodium ion insertion and deinsertion.

Recently, transition metal disulfides and diselenides, such as FeS_2, MoS_2, $FeSe_2$, and $MoSe_2$, have been reported as potential materials for SIBs due to their unique physical, chemical, and electronical properties.[12−19] FeS_2 and MoS_2 both showed a stable discharge capacity of ~200 mAh/g at 1000 mA/g.[12,13] $FeSe_2$ and $MoSe_2$ also displayed a discharge capacity of 372 and 364 mAh/g at 1000 mA/g, respectively.[14,15] Nevertheless, the Coulombic efficiency (CE) of these anode materials in the first cycle is not high. It indicates that there is still much irreversible initial capacity loss in the first galvanostatic cycle. Besides, long-term cycle life of anode materials at high current density for SIBs is still a challenge. $NiSe_2$, which has a comparable band gap energy with good conductivity (resistivity below 10^{-3} Ω cm), is a promising electrode material.[17−24] Face-centered cubic crystal structure of $NiSe_2$ is the most common and usually is classified as a NaCl-like group that Ni and Se_2 atoms correspond to Na and Cl atoms, respectively. As shown in Figure 1b, the Se atoms octahedrally bond to the adjacent Ni atoms.[23] This structure is very stable. Meanwhile, as an anode material, $NiSe_2$ with a conversion mechanism has high theoretical capacity (495 mAh/g). When applied as LIBs anode, it exhibited excellent electrochemical performance.[20] $NiSe_2$, coated with reduced graphene oxide and carbon ($NiSe_2$-rGO-C), when applied as SIBs anode, also displayed good electrochemical properties (274 mAh/g at 1 A/g).[17] However, the complicated fabrication process and unsatisfactory cycle life of $NiSe_2$ cannot meet the requirements of industrial production and demands of commercial energy storage. Therefore, it is challenging, but desirable, to investigate this material as an anode for the large-scale rechargeable SIBs.

Herein, we present a hydrothermal method to prepare $NiSe_2$ nanooctahedra as anode material for SIBs. It shows high specific capacity, long-term cyclic stability (313 mAh/g after 4000 cycles at 5 A/g, 396 mAh/g after 200 cycles at 200 mA/g), and superior rate performance (230 mAh/g at 10 A/g and 175 mAh/g at 20 A/g). Furthermore, the reaction mechanism and the reason for discharge specific capacity decays gradually during the first 50 cycles are first investigated by *in situ* and *ex situ* X-ray diffraction (XRD, different cycle numbers), selected

Received: August 12, 2016
Accepted: December 12, 2016
Published: December 12, 2016

DOI: 10.1021/acsami.6b10143
ACS Appl. Mater. Interfaces 2017, 9, 311−316

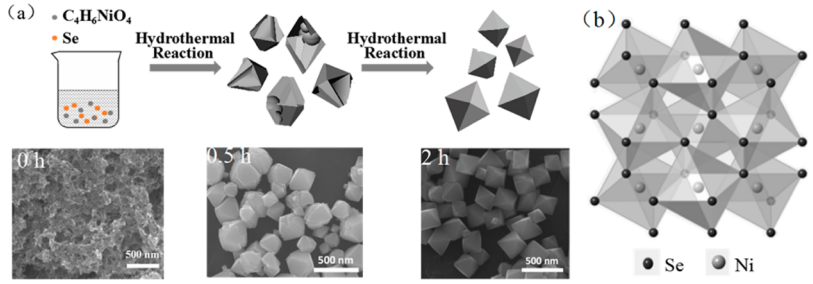

Figure 1. (a) A schematic illustration of forming process of $NiSe_2$ nanooctahedra through one-step hydrothermal method. (b) Crystal structure of pyrite-type $NiSe_2$.

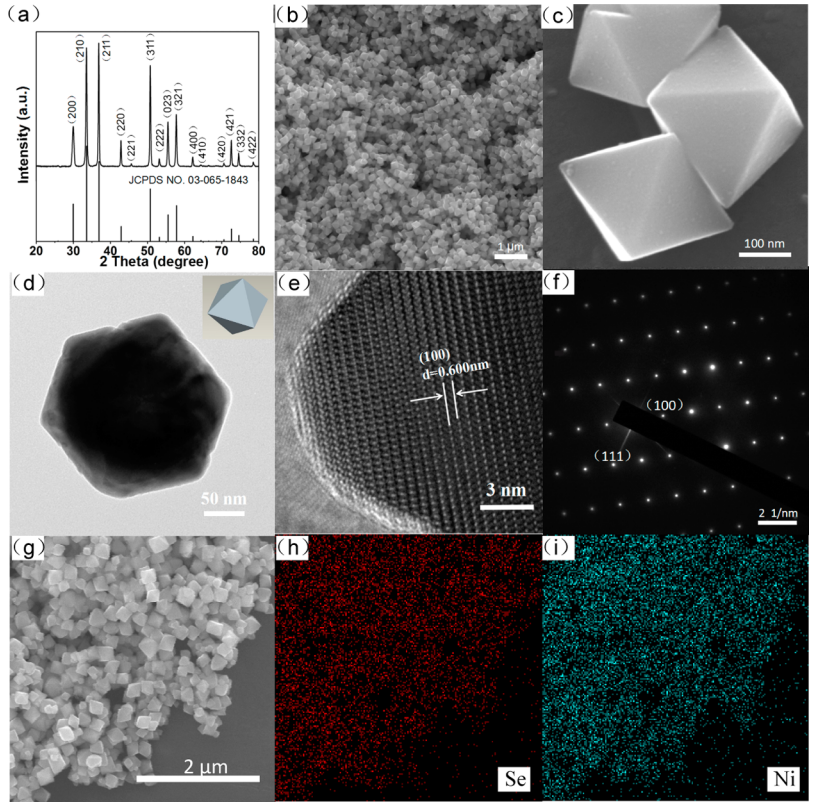

Figure 2. (a) XRD pattern, (b, c) SEM images with different magnifications, (d) TEM image, (e) HRTEM image, (f) SAED pattern, and (g–i) elemental mapping images of the as-prepared $NiSe_2$.

area electron diffraction (SAED), and high-resolution transmission electron microscopy (HRTEM).

EXPERIMENT SECTION

Synthesis of $NiSe_2$ Nanooctahedra. $NiSe_2$ nanooctahedra were synthesized via a hydrothermal method. In brief, 2 mmol of nickel acetate tetrahydrate ($C_4H_6NiO_4{\cdot}4H_2O$, 0.4977 g) and 8 mmol of selenium powder (Se, 0.6312 g) were added into deionized water. Then, 30 mL of $N_2H_4{\cdot}H_2O$ (80%) was added into the mixture drop-by-drop under continuous stirring. After 60 min, the mixture was heated at 140 °C for 20 h in a Teflon bomb. The black $NiSe_2$ crystals were obtained after cooling to room temperature, centrifuging the suspension, and drying.

Material Characterizations. The phase purity, chemical compositions, and crystallographic data of the as-synthesized sample were performed by using a D8 Advance X-ray diffractometer (Rigaku Dmax-RB with Cu Kα X-ray source, Germany). A transmission electron microscope (TEM, JEM-2100F, Japan) and scanning electron microscope (SEM, JSM-7100F, Japan) were used to investigate the morphology and microstructure of the $NiSe_2$.

Electrochemical Measurements. The electrochemical performances of $NiSe_2$ nanooctahedra were measured by assembling 2016 coin cells in an Ar-filled glovebox. The working electrodes consisted of 70 wt % of $NiSe_2$ nanooctahedra, 20 wt % electrical conductor (acetylene black), and 10 wt % carboxyl methyl cellulose (CMC) binder on copper foil. A pure sodium disk was used as counter electrode and a 1.0 M sodium trifluomethanesulfonate ($NaCF_3SO_3$) in diethylene glycol dimethyl ether (DEGDME) as the electrolyte. Galvanostatic charge–discharge tests of as-prepared cells were investigated using the LAND-CT2001A battery test system from 0.3 to 2.9 V.

RESULTS AND DISCUSSION

The process of synthesizing $NiSe_2$ nanooctahedra and the SEM images of different hydrothermal time are shown in Figure 1a. Generally speaking, the inherent crystal structure dominates the final morphology of nanocrystals, especially in inchoate nucleation and subsequent growth stage. Different morphologies of nanocrystals can be synthesized via delicate control of external factors, for example, temperature, reaction time, and surfactants.[25,26] The crystal faces with higher surface energy

DOI: 10.1021/acsami.6b10143
ACS Appl. Mater. Interfaces 2017, 9, 311–316

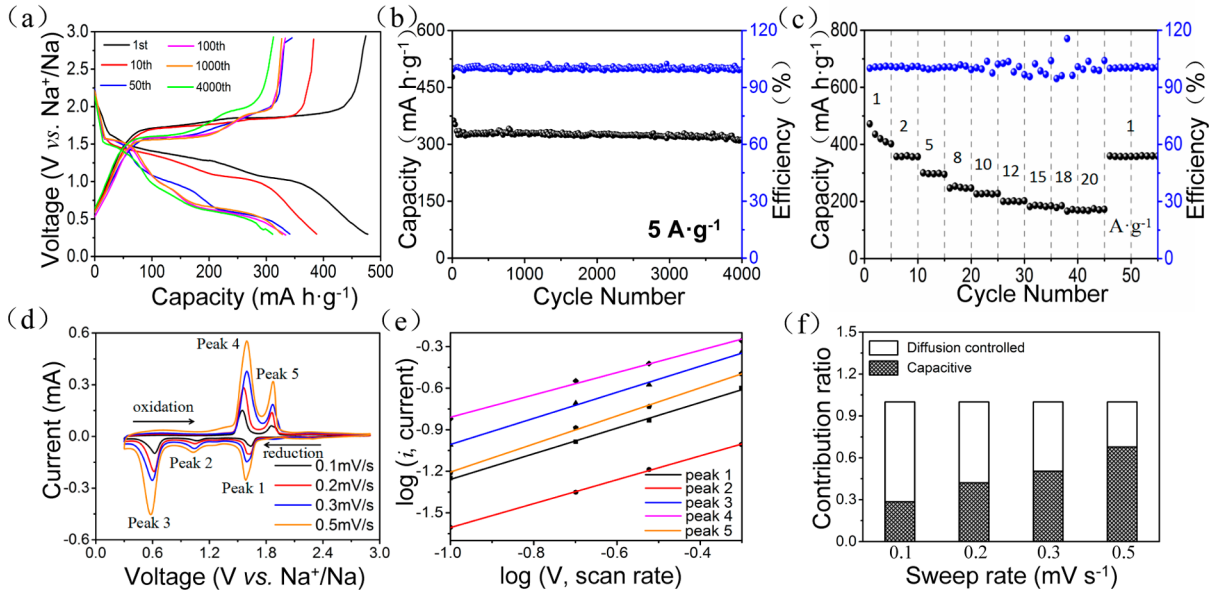

Figure 3. Electrochemical performances of $NiSe_2$ half-cells. (a) Charge−discharge curves, (b) long-term cyclic performance, (c) rate performance, (d) CV curves at different scan rates from 0.1 to 0.5 mV s^{-1} after 100 cycles of the as-prepared $NiSe_2$, (e) log(i) versus log(v) plots, and (f) contribution ratio of the capacitive and diffusion-controlled charge at various scan rates.

tend to disappear along with the growth of crystals. According to Gibbs−Wulff's theorem,[27] growth rate of each crystal face is $\gamma_{\{111\}} < \gamma_{\{100\}} < \gamma_{\{110\}}$ for an intrinsic face-centered cubic $NiSe_2$ crystal. What is more, because the mixed solvents are N_2H_4/H_2O, there are no organic molecules adsorbing on the crystal faces of $NiSe_2$. Thus, the crystal face of {111} grows the slowest and is exposed, leading to the formation of $NiSe_2$ nanooctahedra.

Figure 2a shows the XRD pattern of the $NiSe_2$ sample. All of the diffraction peaks are fully consistent with the standard patterns of $NiSe_2$ (cubic, $Pa\bar{3}$, JCPDS Card No. 03-065-1843). The sharp peaks indicate the good crystallinity of the $NiSe_2$, and there is no impurity can be detected. The morphology and microstructure of $NiSe_2$ are characterized by SEM and TEM. Figure 2b,c shows SEM images of the $NiSe_2$ at different magnifications. The product we obtained is homogeneous $NiSe_2$ nanooctahedra, and the size of $NiSe_2$ is approximately 150−250 nm. A TEM image is shown in Figure 2d. It further indicates that the morphology of as-prepared $NiSe_2$ is a geometric nanooctahedron, which is consistent with SEM observations (Figure 2b,c). The HRTEM image (Figure 2e) of the $NiSe_2$ nanooctahedra exhibits clear 0.600 nm spaced lattice fringes which is indexed to the (100) crystal face of $NiSe_2$ (JCPDS Card No. 03-065-1843). The SAED pattern (Figure 2f) indicates that the $NiSe_2$ nanooctahedra are well-developed single crystals of cubic structure. In addition, the elemental mapping images are shown in Figure 2g−i. They reveal the uniform distribution of the Ni and Se elements throughout the $NiSe_2$ nanooctahedra.

The electrochemical performances of the $NiSe_2$ nanooctahedra for sodium ion storage were tested via fabricating 2016 coin-type cells. The $NaCF_3SO_3$ (1.0 M) in diethylene glycol dimethyl ether (DEGDME) was chosen as electrolyte. In order to avoid deep discharging, we took the voltage window of 0.3−2.9 V into consideration. Figure 3a shows the charge−discharge curves of $NiSe_2$ nanooctahedra at a high constant current density of 5000 mA/g. The initial discharge and charge capacities of $NiSe_2$ are 478 and 469 mAh/g, respectively. This initial CE is more than 95%. Furthermore, the charge−discharge curves are almost overlapped after 50 cycles and stable plateaus are located at 1.55, 1.88 V and at 1.58, 1.05, 0.60 V during the charge and discharge process, respectively. It indicates that $NiSe_2$ nanooctahedra possess excellent cycling stability. Obviously, the charge behavior of the 1st and 10th cycles is different from that after the 50th cycle. The reason for this is that, instead of turning to $NiSe_2$, part of Na_2Se changes into Se and Ni_3Se_4 gradually when charged to 2.9 V during the first 50 cycles.

Figure 3b shows the long-term cycle performance of $NiSe_2$ at 5000 mA/g. The discharge specific capacity still remains at 313 mAh/g after 4000 cycles. Throughout the whole cycle stage, the CE nearly maintains 100%. However, the discharge specific capacity gradually decays during the first 50 cycles. Electrochemical impedance spectra (EIS) are shown in Figure S1. Two compressed semicircles are clearly observed. The diameter of the first semicircle is dominated by solid electrolyte interface (SEI) film, and another is controlled by charge transfer resistance (R_{ct}). Obviously, R_{ct} increases gradually during the first 50 cycles, and it is consistent with the decrease of capacity. The morphology change of the $NiSe_2$ electrode after 50 cycles is shown in Figure S2. As with many transition metal oxides and sulfides, the $NiSe_2$ turns into nanoparticles, which shortens the Na^+ transport path.[14,18]

The cycle performance of $NiSe_2$ at 0.2 A/g was also tested as shown in Figure S3. The initial CE reaches 93%, and the discharge capacity of $NiSe_2$ maintains at 396 mAh/g after 200 cycles. However, the discharge capacity decreases sharply when the voltage was changed from 0.3−2.9 V to 0.01−3 V (Figure S4) and when we used 1 M $NaClO_4$ in 1:1 v/v ethylene carbonate/dimethyl carbonate as electrolyte (Figure S5). All of these results demonstrate that excellent cycle performance and high CE should be ascribed to improve cutoff voltage and select DEGDME as electrolyte.[14,27−30] There is irreversible capacity which mainly comes from the deep discharge from 0.3 to 0 V. Therefore, raising the cutoff voltage appropriately has an active effect on improving CE and cycle performance.[14] In addition,

DOI: 10.1021/acsami.6b10143
ACS Appl. Mater. Interfaces 2017, 9, 311−316

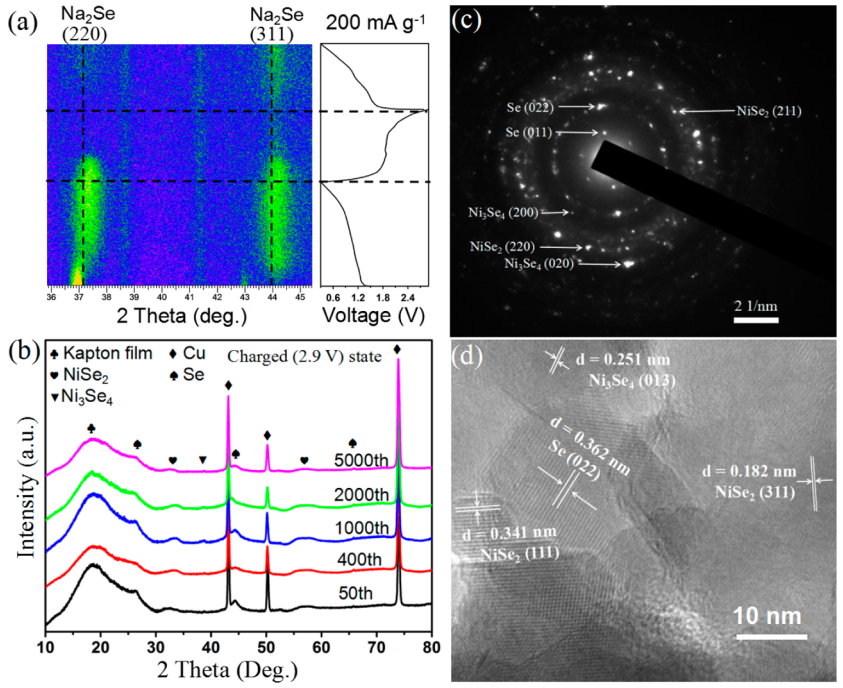

Figure 4. (a) *In situ* XRD patterns collected during the first two discharge/charge cycles at 200 mA/g. (b) XRD patterns of electrodes at charging 2.9 V state after 50, 400, 1000, 2000, 5000 cycles. (c) SAED pattern and (d) HRTRM image of the electrodes at fully charged (2.9 V) state after 2000 cycles.

the use of DEGDME electrolyte has a great influence on superior long-term cyclability because it could avoid the reaction between carbonate-based and anionic groups, which are the charge/discharge products.[12,14] Besides, the cells with DEGDME possess a smaller voltage polarization.[12] Figure 3c shows rate performance of as-prepared $NiSe_2$. Impressively, the electrode of $NiSe_2$ nanooctahedra delivers reversible capacities of 472, 360, 175 mAh/g at 1, 2, 20 A/g, respectively. Due to the formation of SEI film and part of $NiSe_2$ transforms into Ni_3Se_4 and Se with cycling, the capacity decays gradually during the first 5 cycles at 1 A/g.

In order to investigate the possible reasons for the remarkable rate performance, detailed kinetics analysis of the $NiSe_2$ electrode was conducted for sodium ion storage. Cyclic voltammetry (CV) tests at different scan rates from 0.1 to 0.5 mV/s were performed, shown in Figure 3d. The CV curves display similar shapes and with the increase of scan rates, the anodic and cathodic peaks also augment. Two peaks around 1.53 and 1.84 V are clearly observed in the anodic cycle, which correspond to the Na^+ ion deinsertion process. Meanwhile, three peaks around 1.63, 1.08, and 0.62 V are observed in the cathodic cycle, corresponding to the Na^+ ion insertion process. These results are in good agreement with the above charge−discharge profiles after 50 cycles, shown in Figure 3a. In addition, the square root of the scan rate is not proportional to the peak current density, as shown in Figure 3d. In other words, non-Faradaic and Faradaic behaviors control the whole cycle process.[8,14,31,32] The contribution of all stored charge could be analyzed according to the following eq 1 and 2[31,32]

$$i = av^b \tag{1}$$

$$\log(i) = b\log(v) + \log(a) \tag{2}$$

where i is the measured current and v is the scan rate. In particular, power coefficient b is indicative of the charge storage kinetics in the electrode. When the b value approaches 0.5, it indicates that the electrochemical reaction is dominated by ionic diffusion, whereas, when it approaches 1, the capacitive behavior dominates the total process. Figure 3e shows the log i vs log v plots at every peak potential. It clearly demonstrates that the slopes (b value) of peak 1 to peak 5 are 0.93, 0.86, 0.94, 0.81, and 1.01, respectively. These results imply that the electrochemical reaction of $NiSe_2$ nanooctrahedra is mainly controlled by capacitive behavior, which leads to a high-rate performance and extended cycle life. In addition, we further quantified the total capacitive contribution by separating contributions of the capacitive and diffusion-controlled. The relationship $i = av^b$ can be divided into two parts. One is capacitive (k_1v) and another part is diffusion-controlled ($k_2v^{1/2}$), as follows[31,32]

$$i(V) = k_1v + k_2v^{1/2} \tag{3}$$

where k_1 and k_2 are constants. The equation $i(V)/v^{1/2} = k_1v^{1/2} + k_2$ can be obtained by rearranging eq 3, and k_1 is determined as the slope. Therefore, capacitive and diffusion contributions are able to be acquired. Figure 3f indicates that the capacitive contribution turns to dominate gradually with the increase of scan rate. About 68% of total capacity is derived from the capacitive mechanism at 0.5 mV/s. This result also implies the high-rate performance of $NiSe_2$.

The sodium ion storage mechanism of $NiSe_2$ during cycling is further investigated by *in situ* XRD, *ex situ* XRD (different cycle numbers), SAED, and HRTEM. Figure 4a shows *in situ* XRD patterns, and an obvious phase transition could be observed upon electrochemical discharge/charge processes at 200 mA/g. The diffractions at open circuit voltage state are assigned to the $NiSe_2$ phase and they disappear inch-by-inch along with the appearance of two new diffractions at 37.3° and 44.1° which correspond to the (220) and (311) crystal faces of Na_2Se during the first discharge process. However, with the

DOI: 10.1021/acsami.6b10143
ACS Appl. Mater. Interfaces 2017, 9, 311−316

crystalline phase of Na_2Se disappearing, there are no apparent diffractions of $NiSe_2$ in the subsequent cycle process, which may be ascribed to that the particle size of $NiSe_2$ is so tiny. At the second discharge process, Na_2Se appeared again, which demonstrates the reversibility of the electrochemical reaction. Figure 4b shows XRD patterns of electrode material at charging 2.9 V state after 50, 400, 1000, 2000, and 5000 cycles. All of the XRD patterns with different cycle numbers are almost the same, which implies that this electrode material possesses excellent long-term cyclic stability. The characteristic peak of kapton film is located in 19°, and it is used to isolate the electrode from air. The peaks of the current collector (Cu) are obviously found in every pattern of tested samples. Moreover, the peaks of $NiSe_2$ are observed at 33.6° and 57.8° and new peaks are found which are congruent with Se and Ni_3Se_4. In addition, the SAED pattern (Figure 4c) and HRTEM (Figure 4d) also confirm the products when the samples were charged to 2.9 V after cycling for 2000 cycles. As shown in Figure 4c, several discernible concentric rings composed of discrete spots match well with the diffractions of cubic $NiSe_2$, monoclinic Ni_3Se_4, and monoclinic Se. HRTEM investigation in Figure 4d shows resolved lattice fringes of $NiSe_2$ (111) and (311) planes with a spacing of 0.341 and 0.182 nm, and lattice fringes of the Ni_3Se_4 (013) plane with a spacing of 0.251 nm, as well as (022) planes of the neighboring Se support with a spacing of 0.362 nm, respectively. However, as shown in Figure S6, no Ni_3Se_4 and Se can be detected in the electrode at the initial charged states. It may be that there are very few Na_2Se changed into Se and Ni_3Se_4, so the products of Se and Ni_3Se_4 are too few to be detected during the first charging. They can be detected with cycling and the accumulation of Se and Ni_3Se_4.

Combining the above results and previous reports about $FeSe_2$ and $CoSe_2$ anodes for SIBs,[14,18] the reaction mechanism of $NiSe_2$ can be inferred. The three discharge plateaus may indicate the formation of Na_xNiSe_2, NiSe and Na_2Se, and Ni and Na_2Se, respectively.[14,18] The two charge plateaus are corresponding to the formation of Na_xNiSe_2 and fully charged products $NiSe_2$, Se, and Ni_3Se_4, respectively. The reaction equations are summarized below.

Discharge process:

$$\text{Peak 1}\quad NiSe_2 + 2Se + Ni_3Se_4 + 4xNa^+ + 4xe^- \rightarrow 4Na_xNiSe_2 \tag{4}$$

$$\text{Peak 2}\quad Na_xNiSe_2 + (2-x)Na^+ + (2-x)e^- \rightarrow NiSe + Na_2Se \tag{5}$$

$$\text{Peak 3}\quad NiSe + 2Na^+ + 2e^- \rightarrow Ni + Na_2Se \tag{6}$$

Charge process:

$$\text{Peak 4}\quad Ni + 2Na_2Se \rightarrow Na_xNiSe_2 + (4-x)Na^+ + (4-x)e^- \tag{7}$$

$$\text{Peak 5}\quad 4Na_xNiSe_2 \rightarrow NiSe_2 + 2Se + Ni_3Se_4 + xNa^+ + xe^- \tag{8}$$

As a matter of fact, instead of turning to $NiSe_2$, part of Na_2Se changes into Se and Ni_3Se_4 gradually when charged to 2.9 V during the first 50 cycles. That is why the discharge specific capacity decays gradually at that time, according to the *ex situ* XRD patterns (Figure 4b), SAED pattern (Figure 4c), and HRTEM (Figure 4d). After 50 cycles, when electrode material is charged to 2.9 V again, the $NiSe_2$, Se, and Ni_3Se_4 reach a balance and the discharge specific capacity does not decay obviously.

CONCLUSIONS

We have demonstrated a facile approach to prepare $NiSe_2$ nanooctahedra. When used as anode material for SIBs, it exhibits superior electrochemical performances. By tuning the cutoff voltage and selecting DEGDME as the electrolyte, $NiSe_2$ shows good capacity stability (313 mAh/g at 5 A/g after 4000 cycles), high initial CE (above 95%), and superior rate performance (175 mAh/g at 20 A/g). During the charge−discharge processes, the superior rate performance should be ascribed to the pseudocapacitive behavior. Due to generation of Se and Ni_3Se_4 at charged 2.9 V during the first 50 cycles, the discharge specific capacity decays gradually. When $NiSe_2$, Se, and Ni_3Se_4 reach a balance, the capacity almost remains unchanged. These highlights demonstrate that $NiSe_2$ is a promising anode material for SIBs with high-rate performance and long-term cyclability.

ASSOCIATED CONTENT

Supporting Information

The Supporting Information is available free of charge on the ACS Publications website at DOI: 10.1021/acsami.6b10143.

Additional Figures S1−S6. EIS curves of $NiSe_2$ during the first 50 cycles (Figure S1). SEM image of $NiSe_2$ electrode after 50 cycles (Figure S2). Cycling performance of as-prepared $NiSe_2$ at 200 mA/g (Figure S3). Cycling performance of as-prepared $NiSe_2$ at 200 mA/g from 0.01 to 3 V (Figure S4). Cycling performance of as-prepared $NiSe_2$ using 1 M $NaClO_4$ in EC/DEC at 200 mA/g (Figure S5). SAED pattern and HRTRM image of $NiSe_2$ electrode at initial charged to 2.9 V (Figure S6) (PDF)

AUTHOR INFORMATION

Corresponding Authors

*E-mail: wql236@163.com (Q.W.).
*E-mail: mlq518@whut.edu.cn (L.M.).

ORCID

Liqiang Mai: 0000-0003-4259-7725

Author Contributions

The manuscript was written through contributions of all authors and the contributions of Qidong Li are almost equal to the first author's contributions. All authors have given approval to the final version of the manuscript.

Notes

The authors declare no competing financial interest.

ACKNOWLEDGMENTS

This work was supported by the National Key Research and Development Program of China (2016YFA0202603), the National Basic Research Program of China (2013CB934103), the National Natural Science Foundation of China (51521001, 51272197, 51602239), the National Natural Science Fund for Distinguished Young Scholars (51425204), and the Funda-

DOI: 10.1021/acsami.6b10143
ACS Appl. Mater. Interfaces 2017, 9, 311−316

mental Research Funds for the Central Universities (WUT: 2016III001, 2016III003, 2016IVA090).

REFERENCES

(1) Tarascon, J. M.; Armand, M. Issues and Challenges Facing Rechargeable Lithium Batteries. *Nature* **2001**, *414*, 359−367.

(2) Goodenough, J. B.; Kim, Y. Challenges for Rechargeable Li Batteries. *Chem. Mater.* **2010**, *22*, 587−603.

(3) Berthelot, R.; Carlier, D.; Delmas, C. Electrochemical Investigation of the P2-Na_xCoO_2 Phase Diagram. *Nat. Mater.* **2011**, *10*, 74−80.

(4) Yabuuchi, N.; Kajiyama, M.; Iwatate, J.; Nishikawa, H.; Hitomi, S.; Okuyama, R.; Usui, R.; Yamada, Y.; Komaba, S. P2-Type $Na_x[Fe_{1/2}Mn_{1/2}]O_2$ Made From Earth-abundant Elements for Rechargeable Na Batteries. *Nat. Mater.* **2012**, *11*, 512−517.

(5) Cao, Y. L.; Xiao, L. F.; Wang, W.; Choi, D. W.; Nie, Z. M.; Yu, J. G.; Saraf, L. V.; Yang, Z. G.; Liu, J. Reversible Sodium Ion Insertion in Single Crystalline Manganese Oxide Nanowires with Long Cycle Life. *Adv. Mater.* **2011**, *23*, 3155−3160.

(6) Pan, H. L.; Hu, Y. S.; Chen, L. Q. Room-temperature Stationary Sodium-ion Batteries for Large-scale Electric Energy Storage. *Energy Environ. Sci.* **2013**, *6*, 2338−2360.

(7) Goodenough, J. B.; Park, K. S. The Li-Ion Rechargeable Battery: A Perspective. *J. Am. Chem. Soc.* **2013**, *135*, 1167−1176.

(8) Wu, D.; Li, X.; Xu, B.; Twu, N.; Liu, L.; Ceder, G. $NaTiO_2$: A Layered Anode Material for Sodium-Ion Batteries. *Energy Environ. Sci.* **2015**, *8*, 195−202.

(9) Palomares, V.; Serras, P.; Villaluenga, I.; Hueso, K. B.; Carretero-Gonzalez, J.; Rojo, T. Na-ion Batteries, Recent Advances and Present Challenges to Become Low Cost Energy Storage Systems. *Energy Environ. Sci.* **2012**, *5*, 5884−5901.

(10) Islam, M. S.; Fisher, C. Lithium and Sodium Battery Cathode Materials: Computational Insights Into Voltage, Diffusion and Nanostructural Properties. *Chem. Soc. Rev.* **2014**, *43*, 185−204.

(11) Das, S. K.; Lau, S.; Archer, L. A. Sodium-Oxygen Batteries: A New Class of Metal-Air Batteries. *J. Mater. Chem. A* **2014**, *2*, 12623−12629.

(12) Hu, Z.; Zhu, Z.; Cheng, F.; Zhang, K.; Wang, J.; Chen, C.; Chen, J. Pyrite FeS_2 for High-Rate and Long-Life Rechargeable Sodium Batteries. *Energy Environ. Sci.* **2015**, *8*, 1309−1316.

(13) Hu, Z.; Wang, L. X.; Zhang, K.; Wang, J. B.; Cheng, F. Y.; Tao, Z. L.; Chen, J. MoS_2 Nanoflowers with Expanded Interlayers as High-Performance Anodes for Sodium-Ion Batteries. *Angew. Chem., Int. Ed.* **2014**, *53*, 12794−12798.

(14) Zhang, K.; Hu, Z.; Liu, X.; Tao, Z.; Chen, J. $FeSe_2$ Microspheres as a High-Performance Anode Material for Na-Ion Batteries. *Adv. Mater.* **2015**, *27*, 3305−3309.

(15) Ko, Y. N.; Choi, S. H.; Park, S. B.; Kang, Y. C. Hierarchical $MoSe_2$ Yolk−Shell Microspheres with Superior Na-ion Storage Properties. *Nanoscale* **2014**, *6*, 10511−10515.

(16) Yue, J. L.; Sun, Q.; Fu, Z. W. Cu_2Se with Facile Synthesis as a Cathode Material for Rechargeable Sodium Batteries. *Chem. Commun.* **2013**, *49*, 5868−5870.

(17) Cho, J. S.; Lee, S. Y.; Kang, Y. C. First Introduction of $NiSe_2$ to Anode Material for Sodium-Ion Batteries: A Hybrid of Graphene-Wrapped $NiSe_2$/C Porous Nanofiber. *Sci. Rep.* **2016**, *6*, 23338−23347.

(18) Zhang, K.; Park, M.; Zhou, L.; Lee, G.; Li, W.; Kang, Y.; Chen, J. Urchin-Like $CoSe_2$ as a High-Performance Anode Material for Sodium-Ion Batteries. *Adv. Funct. Mater.* **2016**, *26*, 6728−6735.

(19) Park, G. D.; Lee, J. H.; Kang, Y. C. Superior Na-ion Storage Properties of High Aspect Ratio SnSe Nanoplates Prepared by a Spray Pyrolysis Process. *Nanoscale* **2016**, *8*, 11889−11896.

(20) Xue, M.; Fu, Z. Lithium Electrochemistry of $NiSe_2$: A New Kind of Storage Energy Material. *Electrochem. Commun.* **2006**, *8*, 1855−1862.

(21) Liang, J.; Yang, Y.; Zhang, J.; Wu, J.; Dong, P.; Yuan, J.; Zhang, G.; Lou, J. Metal Diselenide Nanoparticles as Highly Active and Stable Electrocatalysts for the Hydrogen Evolution Reaction. *Nanoscale* **2015**, *7*, 14813−14816.

(22) Honig, J. M.; Spałek, J. Electronic Properties of $NiS_{2-x}Se_x$ Single Crystals: From Magnetic Mott−Hubbard Insulators to Normal Metals. *Chem. Mater.* **1998**, *10*, 2910−2929.

(23) Ogawa, S. Magnetic Properties of 3D Transition-Metal Dichalcogenides with the Pyrite Structure. *J. Appl. Phys.* **1979**, *50*, 2308−2311.

(24) Qu, C.; Jiao, Y.; Zhao, B.; Chen, D.; Zou, R.; Walton, K. S.; Liu, M. Nickel-Based Pillared MOFs for High-Performance Supercapacitors: Design, Synthesis and Stability Study. *Nano Energy* **2016**, *26*, 66−73.

(25) Lee, S. M.; Cho, S. N.; Cheon, J. Anisotropic Shape Control of Colloidal Inorganic Nanocrystals. *Adv. Mater.* **2003**, *15*, 441−444.

(26) Du, W. M.; Qian, X. F.; Niu, X. S.; Gong, Q. A. Symmetrical Six-Horn Nickel Diselenide Nanostars Growth From Oriented Attachment Mechanism. *Cryst. Growth Des.* **2007**, *7*, 2733−2737.

(27) Darwiche, A.; Marino, C.; Sougrati, M. T.; Fraisse, B.; Stievano, L.; Monconduit, L. Better Cycling Performances of Bulk Sb in Na-Ion Batteries Compared to Li-Ion Systems: An Unexpected Electrochemical Mechanism. *J. Am. Chem. Soc.* **2012**, *134*, 20805−20811.

(28) Xu, Y.; Zhu, Y.; Liu, Y.; Wang, C. Electrochemical Performance of Porous Carbon/Tin Composite Anodes for Sodium-Ion and Lithium-Ion Batteries. *Adv. Energy Mater.* **2013**, *3*, 128−133.

(29) Kim, H.; Hong, J.; Park, Y.; Kim, J.; Hwang, I.; Kang, K. Sodium Storage Behavior in Natural Graphite using Ether-Based Electrolyte Systems. *Adv. Funct. Mater.* **2015**, *25*, 534−541.

(30) Zhang, N.; Han, X. P.; Liu, Y. C.; Hu, X. F.; Zhao, Q.; Chen, J. 3D Porous γ-Fe_2O_3@C Nanocomposite as High-Performance Anode Material of Na-Ion Batteries. *Adv. Energy Mater.* **2015**, *5*, 1401123−1401129.

(31) Lim, E.; Jo, C.; Kim, H.; Kim, M.; Mun, Y.; Chun, J.; Ye, Y.; Hwang, J.; Ha, K.; Roh, K. C.; Kang, K.; Yoon, S.; Lee, J. Facile Synthesis of Nb_2O_5@Carbon Core−Shell Nanocrystals with Controlled Crystalline Structure for High-Power Anodes in Hybrid Supercapacitors. *ACS Nano* **2015**, *9*, 7497−7505.

(32) Zhu, Y.; Peng, L.; Chen, D.; Yu, G. Intercalation Pseudocapacitance in Ultrathin $VOPO_4$ Nanosheets: Toward High-Rate Alkali-Ion-Based Electrochemical Energy Storage. *Nano Lett.* **2016**, *16*, 742−747.

DOI: 10.1021/acsami.6b10143
ACS Appl. Mater. Interfaces 2017, 9, 311−316